

Defective proteasome biogenesis into skin fibroblasts isolated from Rett syndrome subjects with MeCP2 non-sense mutations

Diego Sbardella^a, Grazia Raffaella Tundo^b, Vincenzo Cunsolo^c, Giuseppe Grasso^c, Raffaella Cascella^{d,e}, Valerio Caputo^{d,e}, Anna Maria Santoro^f, Danilo Milardi^f, Alessandra Pecorelli^{g,h}, Chiara Ciaccio^b, Donato Di Pierro^b, Silvia Leoncini^{i,k}, Luisa Campagnolo^d, Virginia Pironi^d, Francesco Oddone^a, Priscilla Manni^j, Salvatore Foti^c, Emiliano Giardina^{d,e}, Claudio De Felice^k, Joussef Hayek^{k,l}, Paolo Curatolo^d, Cinzia Galasso^d, Giuseppe Valacchi^{g,h}, Massimiliano Coletta^b, Grazia Graziani^m, Stefano Marini^{b,*}

^a IRCSS-Fondazione GB Bietti, Via Livenza, 3, 00198 Rome, Italy

^b Dept of Clinical Sciences and Translational Medicine, University of Rome Tor Vergata, Rome, Italy

^c Department of Chemistry, University of Catania, Catania, Italy

^d Department of Biomedicine and Prevention, University of Rome Tor Vergata, Italy

^e Molecular Genetics Laboratory UILDM, Santa Lucia Foundation, Rome, Italy

^f Institute of Crystallography, National Research Council, Catania, Italy

^g Department of Life Sciences and Biotechnology, University of Ferrara, Ferrara, Italy

^h Plant for Human Health Institute, North Carolina State University, Kannapolis, NC, USA

ⁱ Child Neuropsychiatry Unit, University Hospital, Azienda Ospedaliera Universitaria Senese (AOUS), Siena, Italy

^j Ophthalmology Unit, St. Andrea Hospital, Faculty of Medicine and Psychology, NEMOS Department, University of Rome "Sapienza", Rome, Italy

^k Neonatal Intensive Care Unit, University Hospital, Azienda Ospedaliera Universitaria Senese (AOUS), Siena, Italy

^l "Isola di Bau", Multi-Specialist Centre, Certaldo (Florence), Italy

^m Department of Systems Medicine, University of Rome Tor Vergata, Rome, Italy

ARTICLE INFO

Keywords:

Rett syndrome
Skin primary fibroblasts
Proteasome
α-Ring
PAC1
PAC2

ABSTRACT

Rett Syndrome (RTT) is a rare X-linked neurodevelopmental disorder which affects about 1: 10000 live births. In > 95% of subjects RTT is caused by a mutation in Methyl-CpG binding protein-2 (MECP2) gene, which encodes for a transcription regulator with pleiotropic genetic/epigenetic activities.

The molecular mechanisms underscoring the phenotypic alteration of RTT are largely unknown and this has impaired the development of therapeutic approaches to alleviate signs and symptoms during disease progression.

A defective proteasome biogenesis into two skin primary fibroblasts isolated from RTT subjects harbouring non-sense (early-truncating) MeCP2 mutations (*i.e.*, R190fs and R255X) is herewith reported. Proteasome is the proteolytic machinery of Ubiquitin Proteasome System (UPS), a pathway of overwhelming relevance for post-mitotic cells metabolism. Molecular, transcription and proteomic analyses indicate that MeCP2 mutations down-regulate the expression of one proteasome subunit, α7, and of two chaperones, PAC1 and PAC2, which bind each other in the earliest step of proteasome biogenesis.

Furthermore, this molecular alteration recapitulates in neuron-like SH-SY5Y cells upon silencing of MeCP2 expression, envisaging a general significance of this transcription regulator in proteasome biogenesis.

1. Introduction

Rett Syndrome (RTT) is a rare X-linked neuro-developmental disorder which affects almost exclusively the female gender (1:10000 live births) [1]. Clinical onset is typically within the first year of life when

girls start to lose cognitive, motor, language and social skills, further developing an autism-like behaviour, which led to prior categorizing of RTT among Autism Spectrum Disorders [1].

In more than 95% of cases, RTT is due to a sporadic mutation in Methyl-CpG binding protein-2 (*MECP2*, Xq28) gene, which encodes a

* Corresponding author.

E-mail address: Stefano.marini@uniroma2.it (S. Marini).

<https://doi.org/10.1016/j.bbadis.2020.165793>

Received 28 December 2019; Received in revised form 6 March 2020; Accepted 4 April 2020

Available online 08 April 2020

0925-4439/ © 2020 Elsevier B.V. All rights reserved.

transcriptional repressor/activator with pleiotropic epigenetic activities [2–4]. In heterozygous females, random X Chromosome Inactivation (XCI) generates a mosaicism of cells expressing wild-type (*wt*) or the mutated MeCP2 allele in whole organism, but even though major alterations can be documented also in non-nervous tissues, lack of functional MeCP2 dramatically impairs Central Nervous System development [2–11].

In fact, RTT females display microcephaly, intellectual disability, transient autism-like behaviour, seizures and impaired visual search (in the absence of retina abnormalities), intense eye-gaze and often develop cardiac, respiratory and digestive tract abnormalities, severe scoliosis and hormone disequilibrium [2–13].

The molecular basis of RTT onset and progression are not well characterized, even though a major redox unbalance has been documented in several tissues, including Red Blood Cells (RBCs) [14–24]. However, discovery that rescue of wild-type (*wt*) MeCP2 expression in a mouse model of RTT reverts the pathological phenotype is a strong stimulus to move forward research on MeCP2 biology [25].

It is well known that a critical role in CNS homeostasis is played by the Ubiquitin Proteasome System (UPS), a major intracellular proteolytic pathway which surveys the proteostasis network, *i.e.* the delicate equilibrium between protein synthesis, folding, trafficking and degradation [26,27].

Proteasome, the core machinery of UPS, is a multi-subunit proteolytic complex which degrades intracellular proteins tagged with a poly-ubiquitin chain (poly-Ub) by E1-E2-E3 enzymes. Proteasome structure is made up by ~56 subunits arranged into two particles, 19S (Regulatory Particle, RP) and 20S (Core Particle, CP) [26,27]. 19S can be divided into two modules, lid and base, which couple the recognition of poly-Ub substrates with their ATP-dependent unfolding before grasping and pulling them into the catalytic chamber of 20S [28–30].

20S is a hollow cylinder-shaped assembly made up by four stacked rings, two outer α and two inner β rings, each composed by seven repeated subunits called α 1–7 (*i.e.*, *PSMA*1–7 genes) and β 1–7 (*i.e.*, *PSMB*1–7 genes) [26–29]. Whilst α -rings interact with 19S and are involved in the allosteric regulation of 20S gate opening and closure, β -rings host the catalytic subunits (*i.e.*, chymotrypsin-like, trypsin-like and caspase-like).

Molecular insights of 19S biogenesis are largely unknown yet, whereas 20S biogenesis pathway has been unveiled by pioneering researches of several authors [31–37]. According to latest findings, α 4 (*i.e.*, *PSMA*7, 20q13.3), α 5 (*i.e.*, *PSMA*5, 1p13.3), α 6 (*i.e.*, *PSMA*1, 11p15.2) and α 7 (*i.e.*, *PSMA*3, 14q23.1) subunits assemble first to form a core α -ring tetrameric intermediate (α 4– α 7) assisted by two chaperones called PAC3 (*i.e.*, *PSMG*3, 7p22.3) and PAC4 (*i.e.*, *PSMG*4, 6p25.2) [37]. Thereafter, two additional chaperones, called PAC1 (*i.e.*, *PSMG*1, 21q22.2, also known as Down Syndrome Critical region 2) and PAC2 (*i.e.*, *PSMG*2, 18p11.21, also known as hepatocellular carcinoma associated gene 3) bind the α -ring intermediate preventing its possible off-pathway dimerization and aggregation which is favoured by α -subunits sticky properties [36,37]. Additionally, PAC1 and PAC2 mediate the recruitment of α 1 (*i.e.*, *PSMA*6, 14q13.2), α 2 (*i.e.*, *PSMA*2, 7p14.1) and α 3 (*i.e.*, *PSMA*4, 15q25.1) subunits, thus leading to the formation of a mature heptameric α -ring [36,37]. This α -ring is then a scaffold for subsequent insertion of the seven β -subunits through contribution of another chaperon, called POMP, to constitute the half-20S molecule at the Endoplasmic Reticulum (ER) outer surface [38]. Two half-proteasomes finally assemble into a mature 20S. Once mature, 19S and 20S may assemble in the cell cytosol, leading to the formation of three main proteasome particles, namely (i) uncapped 20S, (ii) singly capped 26S (19S::20S), and (iii) doubly capped 30S (19S::20S::19S). These particles can be further decorated by Proteasome Interacting Proteins (PIPs) which modulate their composition and proteolytic specificities [25,26,39–41]. However, capped particles are thought to deal with the degradation of poly-Ub proteins, whereas uncapped 20S is supposed to clear unfolded and oxidized proteins regardless the Ub tag [41,42,43].

In a previous paper, mRNAs coding for canonical 19S and 20S forms were found up-regulated in lympho-monocytes isolated from RTT subjects along with a generic reduction in proteasome bulk proteolytic activity [14]. However, this contradictory result between transcriptional regulation of proteasome subunits and proteolytic activity of mature particles was no further investigated.

Herewith, we report that skin primary fibroblasts isolated from RTT patients harbouring two non-sense *MECP2* mutations (*i.e.* R190fs and R255X) are defective in proteasome biogenesis through down-regulated expression of *PSMA*3 (*i.e.*, α 7 subunit), *PSMG*1 (*i.e.*, PAC1 chaperone) and *PSMG*2 (*i.e.*, PAC2 chaperone) genes. Furthermore, defective proteasome biogenesis recapitulates in human neuron-like SH-SY5Y cells upon silencing of MeCP2 expression, envisaging an unprecedented role of MeCP2 in transcriptional regulation of proteasome biogenesis.

2. Results

2.1.1. Reduced content of mature proteasome particles in RTT fibroblasts

Structural and proteolytic properties of intact proteasome particles of skin primary fibroblasts of RTT and healthy subjects were first assayed by native gel electrophoresis [44].

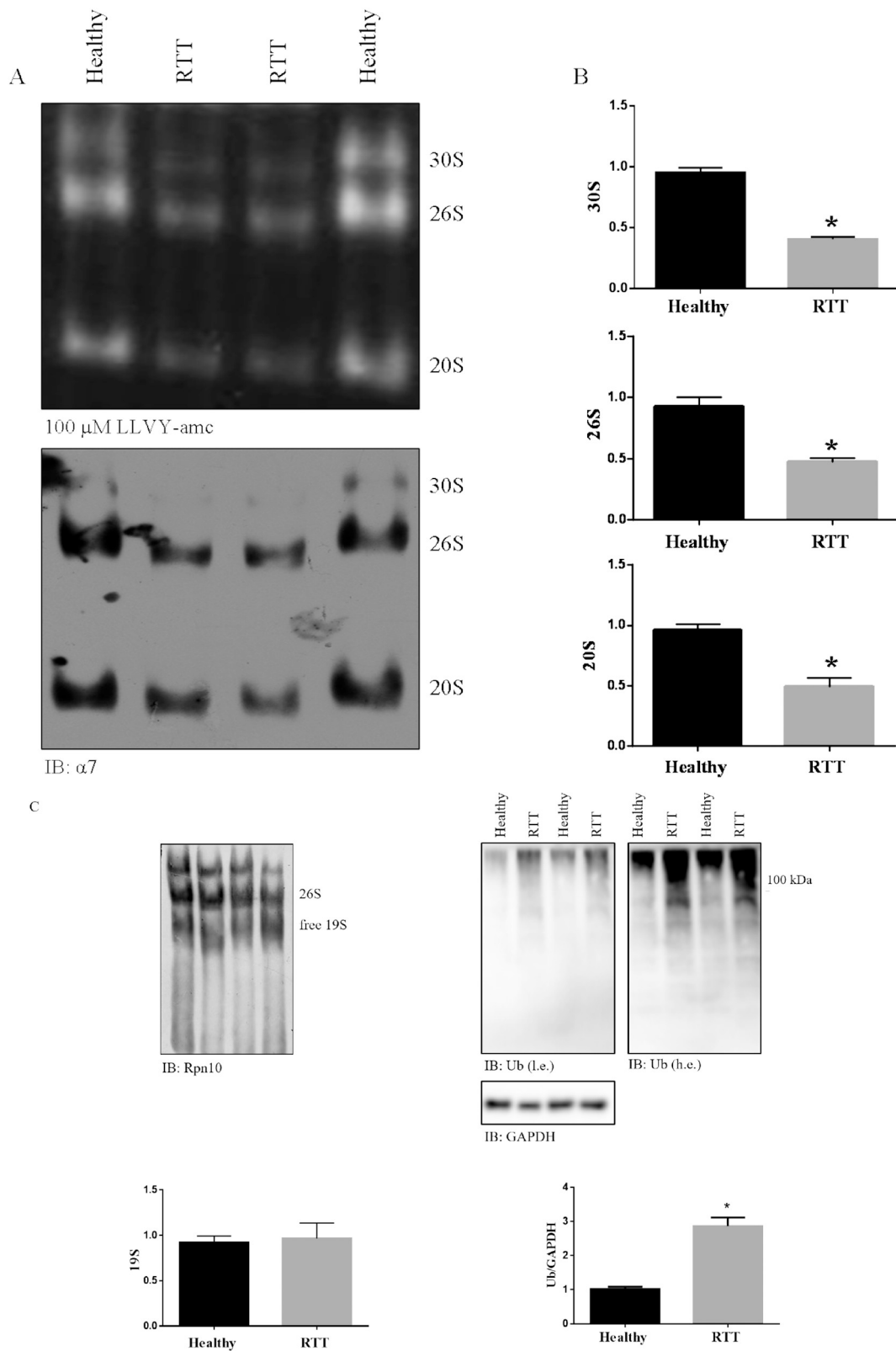
Crude cell extracts (*e.g.*, cytosol fractions) of cells were separated by their molecular mass/charge ratio under non-denaturing conditions and capped (*i.e.* 30S and 26S) and uncapped (*i.e.* free 20S) particles were visualized by probing the gel with 100 μ M Suc-LLVY-amc (*i.e.* LLVY-amc), a fluorogenic substrate specific for chymotrypsin-like activity (Fig. 1A). The cleavage rate of LLVY-amc (which is almost linear with light intensity of each band) of either capped (*i.e.* 30S and 26S) and uncapped (*i.e.* 20S) assemblies of RTT cells were significantly slower than those of healthy cells (Fig. 1A).

To further assess identity, particles were transferred to a nitrocellulose filter and probed with an anti- α 7 subunit of 20S proteasome (being a subunit shared by all assemblies investigated) by Western blotting (WB). Again, immuno-detection of 30S, 26S and 20S was significantly decreased in RTT fibroblasts (Fig. 1B). Capped particles outcome was confirmed by probing the filters with an antibody raised against the Rpn10 (*i.e.* *PSMD*4, 1q21.3) subunit of 19S. This staining further highlighted a free 19S content comparable between RTT and healthy cells (Fig. 1C).

Thereafter, poly-Ub proteins in whole cell extracts were assayed by denaturing and reducing WB. High molecular weight (> 100 kDa) poly-Ub proteins, which are the *bona fide* proteasome substrates, were accumulated in RTT fibroblasts (Fig. 1D).

2.1.2. Identification of an aberrant 20S precursor intermediate in RTT fibroblasts

Upon further staining of the native gel (as in Fig. 1) by Coomassie Brilliant Blue (CBB) to visualize non-catalytic proteasome precursor assemblies a major uncommon band, hereafter referred to as “unidentified band”, with a theoretical mass around 250 kDa, was exclusively visualized in crude cell extracts of RTT fibroblasts (Fig. 2). According to knowledge on proteasome structural properties, this species was suggested to represent an assembly intermediate. Hence, it was excised and subjected to trypsin digestion, mass spectrometry (MS) analysis and database search. MS analysis detected all 20S α -subunits with the exception of α 7 subunit (Table I), showing an apparent predominance of α 4 and α 5 subunits. Remarkably, the missed detection of α 7 subunit was unlikely due to extensive post-translational modification, as the search of all possible modifications provided no results. Most notably, MS analysis highlighted the lack of 20S β -subunits. In this band, some 19S subunits, mostly belonging to base sub-module were further identified; this occurrence was likely attributable to the co-segmentation within the same molecular weight range of 19S assembly intermediates which are not directly bound α -subunits (see Table I).



(caption on next page)

Fig. 1. (A) Native gel electrophoresis of proteasome particles isolated from healthy and RTT fibroblasts under non-denaturing conditions (crude cell extracts) ($n = 2$ for both groups). Proteolytic active particles were probed with 100 μM LLVY-amc and visualized into a Chemidoc gel analyzer (upper panel) (Exc. 365 nm; Em. Visible). Average Molecular Mass of assemblies is 2500 kDa for 30S, 1800 kDa for 26S and 750 kDa for 20S. Identity of proteasome particles was verified by probing the filter with an antibody raised against $\alpha 7$ subunit (lower panel); (B) Densitometric analysis of proteasome bands as they appear in immuno-blot: data are expressed as Mean \pm SEM of three independent observations. A nominal value of 1 was assigned to the intensity of the particle-specific signal of first Healthy cell. 30S: Healthy 0.95 ± 0.021 , RTT 0.4050 ± 0.010 , $*p < 0.0001$; 26S: Healthy 0.9225 ± 0.038 , RTT 0.4725 ± 0.0160 , $*p < 0.0001$; 20S: Healthy 0.9625 ± 0.0225 , RTT 0.4925 ± 0.03544 , $*p < 0.0001$. Unpaired τ Student's test; (C) Identity of proteasome particles was further probed with an anti-Rpn10 antibody; Densitometric analysis of free 19S (bottom panel). A nominal value of 1 was assigned to the intensity of the particle-specific signal of first Healthy cell: Healthy 0.9200 ± 0.03651 , RTT 0.9650 ± 0.08568 . (D) Poly-ubiquitinated proteins in whole cell extracts of Healthy and RTT fibroblasts by denaturing and reducing WB. Filters are presented both as low and high exposure. Densitometric analysis was limited to smear of high molecular weight species (> 100 kDa) which represent the *bona fide* proteasome substrates. A nominal value of 1 was assigned to the intensity of the particle-specific signal of first Healthy cell: Healthy 0.9200 ± 0.03651 , RTT 1.600 ± 0.07071 , $*p < 0.0001$.

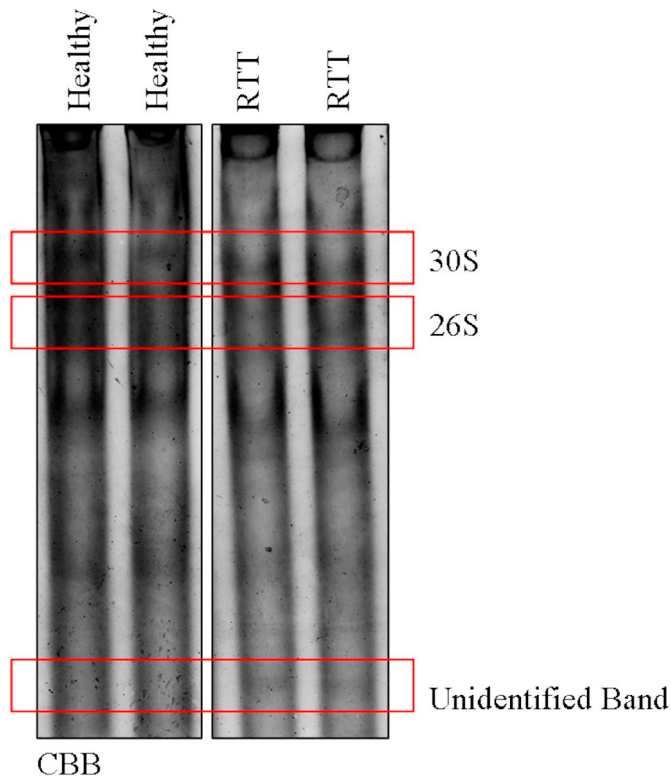


Fig. 2. Identification of an aberrant α -ring intermediate assembly in RTT fibroblasts. Native gel was stained by CBB. Bands within the red rectangular boxes, corresponding, from the top to the bottom of the lane, to 30S, 26S and unidentified band, were excised, digested with porcine trypsin and analyzed by MS (Table I). Area containing 26S and 30S assemblies was excised by following indication of proteolytic activity through overlay assay.

To verify specificity of $\alpha 7$ loss in the “unidentified band”, gel areas containing mature 26S and 30S (labeled in red) were further excised. Notably, 30S and 26S species were confirmed to be less represented in RTT fibroblasts also through CBB staining, which provides a reliable quantitative analysis. MS analysis of 30S and 26S allowed to identify all canonical 19S and 20S subunits, including $\alpha 7$, carrying only very small differences in post-translational modifications as well as some polymorphisms in individual subunits among samples (Suppl. Info Tables I, II).

2.1.3. Selective down-regulation of $\alpha 7$, PAC1 and PAC2 in RTT fibroblasts

To get deeper details on a putative defective proteasome biogenesis, a semi-quantitative analysis of individual 19S and 20S subunits in whole cell extracts of RTT and healthy fibroblast by denaturing and reducing WB was carried out.

In accord with MS analysis, $\alpha 7$ was robustly decreased in RTT fibroblasts together with $\alpha 4$ (Fig. 3A, B). Conversely, $\alpha 2$ content in RTT cells was comparable to that of healthy fibroblasts (Fig. 3A, B).

Thereafter, analysis was extended to 19S subunits, either belonging to lid, namely Rpn7 (*i.e.* PSMD6, 3p14.1) and Rpn10, and base, namely Rpt5 (*i.e.* PSMC3, 11p11.2), and to 20S β -subunits either catalytic $\beta 5$ (*i.e.* PSMB5, 14q11.2) and non-catalytic $\beta 6$ (*i.e.* PSMB1, 6q27). With respect to healthy fibroblasts, all subunits investigated were either over-represented (*i.e.* Rpt5, $\beta 5$, $\beta 6$) in RTT fibroblasts or fully comparable between samples (*i.e.* Rpn10) (Fig. 3A, B).

Thereafter, the expression of PSMA3, PSMA2, PSMA7, PSMB5, PSMB1 and PSMC3 was analyzed by quantitative Real-Time PCR (qPCR). PSMA3 again was severely down-regulated compared to healthy control subjects ($2^{-\Delta\Delta Ct} = 0.53$). The analysis for the remaining genes did not report any considerable differences (Fig. 3C).

Thereafter, to shed light on $\alpha 4$ decrease, expression and abundance of PAC1 and PAC2 chaperones, which assist α -ring formation preventing $\alpha 4$ - $\alpha 7$ core-assembly intermediate aggregation, was assayed by WB and qPCR [31–37].

A very significant decrease in intracellular content of PAC1 and PAC2 in RTT fibroblasts compared to healthy cells was documented (Fig. 3D). According to this result, the expression analysis of PSMG1 (*i.e.* PAC1) and PSMG2 (*i.e.* PAC2) revealed a downregulation with respect to control samples (PSMG1 NM_001261824, NM_003720 $2^{-\Delta\Delta Ct} = 0.29$; PSMG2 $2^{-\Delta\Delta Ct} = 0.75$) (Fig. 3E). To verify specificity of PAC1, PAC2 down-regulation, POMP, which is not involved in α -ring maturation, but in later step of 20S biogenesis was further analyzed [38]: POMP was increased in RTT cells, this being consistent with previous data demonstrating POMP mRNA up-regulation in RTT primary cells (Fig. 3D) [14].

2.1.4. MeCP2 silencing in SH-SY5Y cells recapitulates the defective proteasome biogenesis

To verify whether defective proteasome biogenesis of RTT fibroblasts is a cell-specific phenomenon or else MeCP2 is a more general and unprecedented transcription regulator of proteasome biogenesis, MECP2 expression was silenced in human neuron-like SH-SY5Y cell line upon delivery of 1 μM pool of four MECP2 small-interfering RNAs (*i.e.* siRNAs) (hereafter referred to as treated cells). Treated cells were compared to untreated cells or cells transfected with 1 μM pool of four non-targeting siRNAs (hereafter referred to as scrambled cells). Whole cell lysates and crude cell extracts were harvested after 72 h of stimulation.

Efficient silencing of MECP2 was confirmed by denaturing and reducing WB of whole cell lysates: both ~ 72 and ~ 50 kDa MeCP2 species were markedly reduced in treated cells (Fig. 4A and B). Thereafter, $\alpha 7$, PAC1 and PAC2, but not $\beta 5$ subunit, were found to be significantly reduced in treated cells whereas data of untreated and scrambled cells were comparable (Fig. 4A and B).

Finally, analysis of crude cell extracts of the same experimental groups by native gel electrophoresis showed a marked decrease in mature proteolytic active proteasome particles, either capped or uncapped, in treated cells compared to either untreated or scrambled cells (Fig. 4C).

Accordingly, the poly-ubiquitinated proteins pattern was increased in MeCP2-silenced cells (Fig. 4C).

Table 1

List of the proteasome subunits identified by MS analysis in the bands investigated. Green and red boxes indicate the presence or the absence of the subunit, respectively. Details about the results of database searching are reported in the Suppl. Info. section.

Subunit acc. no.	Particle	Proteasome Subunit	Healthy		RTT		
			30S	26S	30S	26S	Unidentified Band
	20S						
sp P25786 PSA1_HUMAN		PSMA1 (α 6)	x	x	x	x	x
sp P25787 PSA2_HUMAN		PSMA2 (α 2)	x	x	x	x	x
sp P25788 PSA3_HUMAN		PSMA3 (α 7)	x	x	x	x	
sp P25789 PSA4_HUMAN		PSMA4 (α 3)	x	x	x	x	x
sp P28066 PSA5_HUMAN		PSMA5 (α 5)	x	x	x	x	x
sp P60900 PSA6_HUMAN		PSMA6 (α 1)	x	x	x	x	x
sp O14818 PSA7_HUMAN		PSMA7 (α 4)	x	x	x	x	x
sp P20618 PSB1_HUMAN		PSMB1 (β 6)	x	x	x	x	
sp P49721 PSB2_HUMAN		PSMB2 (β 4)	x	x	x	x	
sp P49720 PSB3_HUMAN		PSMB3 (β 3)	x	x	x	x	
sp P28070 PSB4_HUMAN		PSMB4 (β 7)	x	x	x	x	
sp P28074 PSB5_HUMAN		PSMB5 (β 5)	x	x	x	x	
sp P28072 PSB6_HUMAN		PSMB6 (β 1)	x	x	x	x	
sp Q99436 PSB7_HUMAN		PSMB7 (β 2)	x	x	x	x	
sp P28062 PSB8_HUMAN		PSMB8 (β 5i)	x	x	x	x	
sp P28065 PSB9_HUMAN		PSMB9 (β 1i)	x				
sp P40306 PSB10_HUMAN		PSMB10 (β 2i)	x		x		
	19S						
sp P62191 PRS4_HUMAN		PSMC1 (Rpt2)	x	x	x	x	x
sp P35998 PRS7_HUMAN		PSMC2 (Rpt1)	x	x	x	x	x
sp P17980 PRS6A_HUMAN		PSMC3 (Rpt5)	x	x	x	x	x
sp P43686 PRS6B_HUMAN		PSMC4 (Rpt3)	x	x	x	x	x
sp P62195 PRS8_HUMAN		PSMC5 (Rpt6)	x	x	x	x	
sp P62333 PRS10_HUMAN		PSMC6 (Rpt4)	x	x	x	x	
sp Q99460 PSMD1_HUMAN		PSMD1 (Rpn2)	x	x	x	x	x
sp Q13200 PSMD2_HUMAN		PSMD2 (Rpn1)	x	x	x	x	x
sp O43242 PSMD3_HUMAN		PSMD3 (Rpn3)	x	x	x	x	
sp Q15008 PSMD6_HUMAN		PSMD6 (Rpn7)	x	x	x	x	
sp P51665 PSMD7_HUMAN		PSMD7 (Rpn8)	x	x	x	x	
sp P48556 PSMD8_HUMAN		PSMD8 (Rpn12)	x	x	x	x	
sp O00231 PSD11_HUMAN		PSMD11 (Rpn6)	x	x	x	x	
sp O00232 PSD12_HUMAN		PSMD12 (Rpn5)	x	x	x	x	
sp Q9UNM6 PSD13_HUMAN		PSMD13 (Rpn9)	x	x	x	x	
sp O00487 PSDE_HUMAN		PSMD14 (Rpn11)	x	x	x	x	
sp P55036 PSMD4_HUMAN		PSMD4 (Rpn10)	x	x	x	x	

3. Discussion

Although *MECP2* is expressed in all human tissues, the impairment of its expression mostly leads to brain alterations, arising the question why neurodevelopment is primarily affected during RTT onset and progression [1,2]. Answer to this point likely encompasses, *i*) higher expression of *MECP2* in neurons than in other cell lineages; *ii*) the possibility that metabolic pathways altered upon *MECP2* loss are of utmost relevance to post-mitotic cells homeostasis. Point *i*) finds some additional clinical support through analysis of retinal tissue which was reported to express a very low amount of MeCP2 and lacks neuro-anatomical or physiological abnormalities in RTT subjects, indeed [12,13]. Conversely, loss of MeCP2 appears to be deleterious for neighbouring Retinal Pigment Epithelium, which could pose a histological basis to explain the late onset of visual decline [45]. This statement renders stimulating the perspective of comparing proteostasis alteration in nervous tissues, such as cortex and retina, in RTT murine models. With reference to point *ii*) several studies support the notion that UPS is of overwhelming relevance to neurons maturation, by driving synaptic formation and pruning, axon sprouting and dendritic spine arborisation, and adult neurons homeostasis [46]. Remarkably, Angelman's Syndrome, which is characterized by signs and symptoms overlapping with those of RTT patients, is caused by a mutation of the

gene coding for an E3 ligase [47,48] and *PSMG1*-KO mice, which display defective proteasome biogenesis, develop diffuse neuroanatomical abnormalities in cortex, hippocampus, dentate gyrus and cerebellum, which are brain areas prominently affected also in RTT subjects [35,49,50].

Herewith, a major defect of proteasome biogenesis has been unveiled into two cultured cell lines of skin primary fibroblasts isolated from RTT subjects harbouring heterozygous non-sense early-truncating mutations of *MECP2* (*i.e.*, R190fs and R255X). In accord with XCI, in these cell cultures only half of cells express the *MECP2* mutated allele, and data refers to an overall pool of *bona fide* healthy (*i.e.*, harbouring no defect in proteasome biogenesis) and sick cells. Hence, it is likely that mature proteasome particles (*i.e.*, 30S, 26S, 20S) stained in RTT fibroblasts proteasome-enriched cell fractions (Fig. 1A) are only those expressed by cells carrying *wt MECP2* allele, whereas cells expressing the mutated allele display a severe lack of these assemblies. This possibility, together with a quick induction of a defective proteasome biogenesis in SH-SY5Y cells upon *MECP2* silencing, an experimental condition which is as close as possible to a *MECP2* early-truncation, further supports the existing knowledge on the relevance of *MECP2* dosage, and loss-of-function indeed, in transcriptional regulation of genes. Notably, relevant proteasome alterations documented here, such as lack of mature proteasome particles and down-regulation of the α 7

subunit were preliminarily observed also in RTT fibroblasts harbouring additional *MECP2* mutations (*i.e.*, T158M, R168X, P152R), even though to a variable extent (data not shown). However, these cell lines stopped replicating before it had been possible to complete the analysis.

Furthermore, it is worth outlining that MeCP2-silenced SH-SY5Y cells display a much less marked loss of mature proteasome assemblies with respect to RTT fibroblasts. However, these observations can be reconciled by taking into account the half-life of proteasome assemblies, which is supposed to be > 1 week in liver cells. Thus, we may speculate that in order to detect a robust drop in proteasome assemblies in SH-SY5Y cells it would have been necessary to grow them in the presence of MeCP2 siRNA over a longer time interval which is, however, incompatible with cell viability in transfection medium.

Molecular defect likely relies on MeCP2-dependent transcriptional down-regulation of *PSMA3* ($2^{-\Delta\Delta Ct} = 0.53$), *PSMG1* (*PSMG1*: $2^{-\Delta\Delta Ct} = 0.29$) and *PSMG2* (*PSMG2*: $2^{-\Delta\Delta Ct} = 0.75$) mRNAs, which impair the α -ring maturation pathway, that is the earliest event in 20S biogenesis [31–37]. As a matter of fact, four independent methodological approaches (*i.e.*, WB, MS, RT-PCR and silencing experiments) have all identified a dys-regulation of these proteins. However, proteomic analyses, either MS and denaturing and reducing WB, provide outcomes of not obvious interpretation also because the fate of free 19S and 20S subunits and of 20S assembly intermediates, which form *in vitro* whenever *PSMG1* and *PSMG2* expression is shut-off, is unclear [31–37]. To compare the data with those reported for *PSMG1*-KO mice might help to draw some insights [35]: in CNS homogenates of this murine

model 19S subunits content was increased, whereas α and β subunits content was decreased; this observation may be put in relation with a decreased half-life of free 20S subunits upon impaired assembly, even though this is a still debated topic [35][51]. In RTT fibroblasts, 19S subunits behaviour recapitulated that observed in *PSMG1*-KO mice; on the other hand, unlike *PSMG1*-KO mice, 20S free β -subunits increased in RTT fibroblasts, this being compatible with their long-half life. Concerning free α -subunits, the occurrence of a decrease of $\alpha 4$ subunit, in the absence of a *PSMA7* (*i.e.*, the $\alpha 4$ gene) transcriptional down-regulation, envisages the possibility that this subunit is sequestered upon aggregation of an α -ring intermediate assembly. This possibility may be somewhat reinforced by the evidence that the stoichiometry of this subunit is increased, together with that of the $\alpha 5$ subunit, in the “unidentified band” of RTT fibroblasts which is likely an aberrant off-pathway assembly. Formation of aberrant $\alpha 4$ - $\alpha 7$ subunits aggregates in *PSMG1*-silenced HEK human cells was actually documented, providing a rationale to this working hypothesis. Furthermore, disordered assemblies of α -subunits with theoretical masses compatible with those observed in RTT fibroblasts were identified in the presence of simultaneous silencing of *PSMG1* with either *PSMA2* (*i.e.*, the $\alpha 2$ subunit), *PSMA6* (*i.e.*, the $\alpha 1$ subunit) or *PSMA4* (*i.e.*, the $\alpha 3$ subunit), but this occurrence was unexplored in the case of *PSMG1* and *PSMA3* (*i.e.*, the $\alpha 7$ subunit) in HEK cells [37]. Hence, detection of six out of seven α -subunits should allow interpreting the “unidentified band” as an attempt of RTT fibroblasts to build up the α -ring and missed detection of only $\alpha 7$ envisages the possibility that its availability may be severely

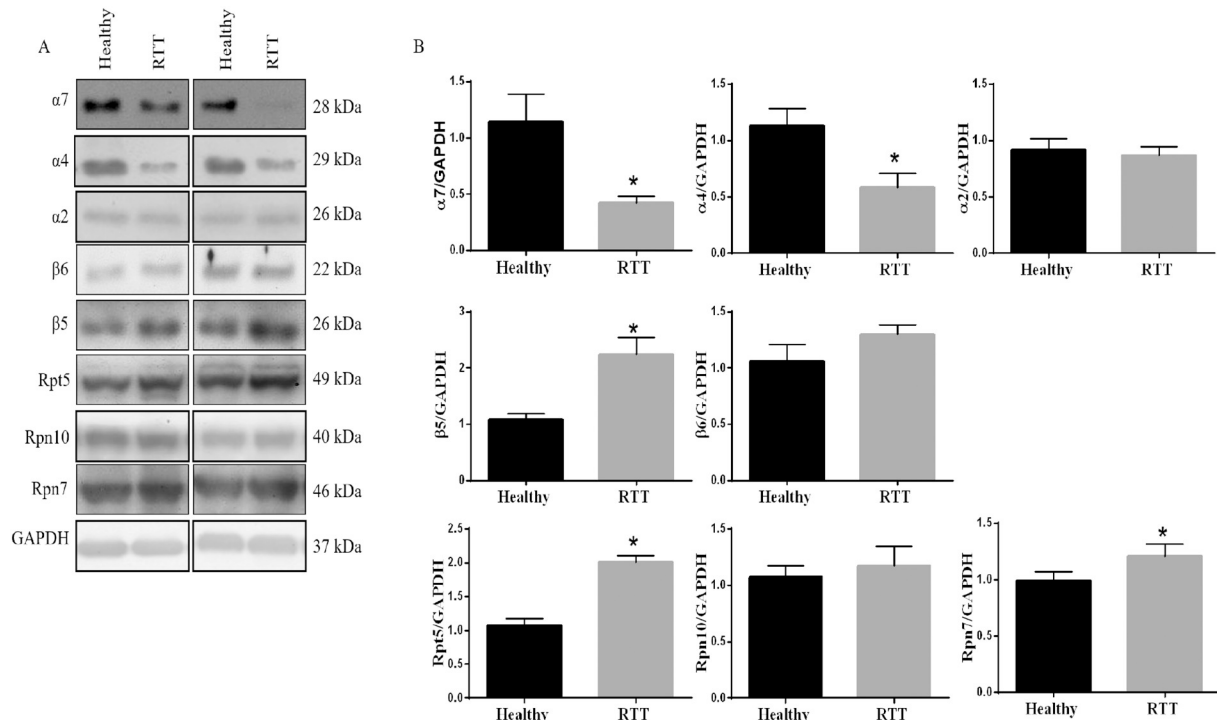


Fig. 3. (A) Semi-quantitative analysis of proteasome subunits in whole cell extracts of Healthy and RTT fibroblasts by denaturing and reducing WB. GAPDH was used as internal control. (B) Densitometric analysis of each subunit is reported on the right. Data are expressed as Mean \pm SEM ($n = 8$ for both healthy and RTT fibroblasts). A nominal value of 1 was assigned to the protein/GAPDH ratio of the first Healthy cell. $\alpha 7$: Healthy 1.145 ± 0.122 , RTT 0.4250 ± 0.027 , $*p < 0.0007$; $\alpha 4$: Healthy 1.125 ± 0.078 , RTT 0.5825 ± 0.663 $*p < 0.00066$; $\alpha 2$: Healthy 0.9150 ± 0.051 , RTT 0.8625 ± 0.04 ; $\beta 5$: Healthy 1.078 ± 0.0539 , RTT 2.238 ± 0.1489 $*p < 0.0034$; $\beta 6$: Healthy 1.058 ± 0.075 , RTT 1.298 ± 0.0043 , $*p < 0.0091$; Rpt5: Healthy 1.070 ± 0.05 , RTT 2.005 ± 0.045 , $*p < 0.0006$; Rpn10: Healthy 1.023 ± 0.04213 , RTT 1.170 ± 0.087 ; Rpn7: Healthy 0.987 ± 0.042 , RTT 1.203 ± 0.096 , $*p < 0.0054$. (C) Quantitative analysis of *PSMA3* (*i.e.* $\alpha 7$), *PSMA2* (*i.e.* $\alpha 2$), *PSMA7* (*i.e.* $\alpha 4$), *PSMB1* (*i.e.* $\beta 6$), *PSMB5* (*i.e.* $\beta 5$), *PSMC3* (*i.e.* Rpt5) expression in Healthy and RTT fibroblasts ($n = 2$ for both groups) by qPCR and comparative $2^{-\Delta\Delta Ct}$ method. Data are expressed by Mean \pm SEM. (D) Semiquantitative analysis of PAC1, PAC2 and POMP in whole cell extracts of healthy and RTT fibroblasts by denaturing and reducing WB ($n = 2$ for both groups). Data are expressed as Mean \pm SD ($n = 8$ for both healthy and RTT fibroblasts). A nominal value of 1 was assigned to the protein/GAPDH ratio of the first Healthy cell. PAC1: Healthy 0.99 ± 0.034 , RTT 0.1650 ± 0.025 , $*p < 0.0001$; PAC2: Healthy 0.98 ± 0.004 , RTT 0.2750 ± 0.044 , $*p < 0.0001$; POMP: Healthy 0.7625 ± 0.09 , RTT 1.027 ± 0.07 , $*p < 0.0001$. Statistical analysis: Unpaired t Student's test. (E) Quantitative analysis of *PSMG1* (*i.e.* PAC1) and *PSMG2* (*i.e.* PAC2) expression in Healthy and RTT fibroblasts by qPCR and comparative $2^{-\Delta\Delta Ct}$ method. Data are expressed by Mean \pm SEM.

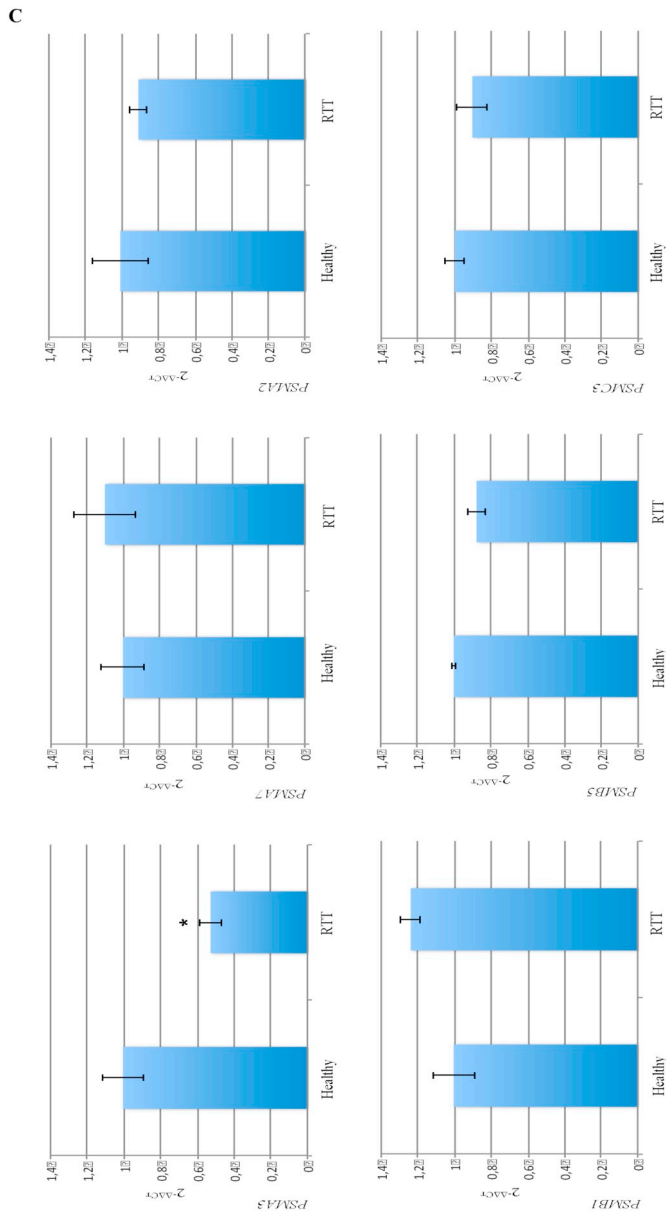


Fig. 3. (continued)

affected not only upon transcription down-regulation but through further post-translational mechanisms [52].

However, to further investigate α -ring biogenesis goes beyond the aim of the present study. Moreover, the limited growth capacity of RTT fibroblasts would not allow to perform more detailed molecular analyses. Furthermore, it is worth recalling that RTT fibroblasts suffer from multiple metabolic alterations, including severe redox unbalance, which supposedly hinders dynamics of proteasome biogenesis pathway leading to pathogenic off-pathway events hard to be replicated in non-RTT cell lines. In addition, it cannot be ruled out that additional post-transcriptional or post-translational mechanisms of regulation of α -subunits and of maturation chaperones, including those not-investigated in this paper, such as PAC3 and PAC4, may actually occur in RTT fibroblasts. With respect to this, MeCP2 regulates microRNAs pathways, and this possibility should be also taken into consideration to find a molecular rationale of *PSMA3*, *PSMG1*, *PSMG2* transcriptional down-regulation [53].

To definitively determine whether this alteration occurs also in living neurons is the greatest achievement of our investigation, giving a possible answer to the question as to whether proteasome biogenesis is

a major pathogenetic event in RTT onset.

Data on *PAC1*-KO mice referenced above and the significant increase in ubiquitin (Ub) immuno-staining in all layers of cerebellum sections of *MeCP2/y^{Tm1.1Bird}* RTT mouse during the transition from the asymptomatic to the symptomatic stage of the disease support this possibility [24]. Although it cannot be exclusively attributed to proteasome impairment, but also to autophagy dys-regulation, a pathological condition hinted in a previous paper by these authors, the enhanced Ub-staining provides a significant clue for a defective proteostasis in CNS during RTT progression.

Hence, together with CANDLE/PRAAS4 syndrome, for which mutations in the promoter of *POMP* and *PSMG2* genes have been identified [54,55], RTT syndrome might hold the requisite of a human pathology determined, at least as a concurrent cause, by altered proteostasis through defective proteasome biogenesis.

As a whole, these data might further be of general relevance in proteasome biology, providing a clue for investigating transcriptional regulation of proteasome genes expression (which is a largely unexplored topic), and for a better knowledge of molecular insights of proteasome proteolytic activity in living cells.

Based on the recent advances in UPS-related pharmacology and considering the challenges of *MECP2* gene therapy, currently regarded as the only therapeutic approach potentially capable of reverting the RTT phenotype, modulation of proteasome activity might provide a novel therapeutic opportunity worth investigating to delay disease progression.

Nonetheless, the very recent enrolment of RTT subjects in a phase II clinical trial run with a drug which stimulates autophagy, whose dys-regulation in the syndrome has been hinted in a previous paper by our group, stimulate the interest in developing proteostasis-rescuing strategies for the clinical management of this disorder [24,56].

Supplementary data to this article can be found online at <https://doi.org/10.1016/j.bbadis.2020.165793>.

CRedit authorship contribution statement

Diego Sbardella: Conceptualization, Investigation, Writing - original draft, Writing - review & editing. **Grazia Raffaella Tundo**: Conceptualization, Investigation, Writing - original draft, Writing - review & editing. **Vincenzo Cunsolo**: Investigation, Formal analysis, Resources. **Giuseppe Grasso**: Investigation, Formal analysis. **Raffaella Cascella**: Investigation, Formal analysis. **Valerio Caputo**: Investigation, Formal analysis, Resources. **Anna Maria Santoro**: Investigation, Formal analysis. **Danilo Milardi**: Investigation, Formal analysis. **Alessandra Pecorelli**: Investigation, Formal analysis. **Chiara Ciaccio**: Investigation, Formal analysis. **Donato Di Piero**: Investigation, Formal analysis. **Silvia Leoncini**: Investigation, Formal analysis. **Luisa Campagnolo**: Investigation, Formal analysis. **Virginia Pironi**: Resources, Investigation. **Francesco Oddone**: Resources, Investigation. **Priscilla Manni**: Resources, Investigation. **Salvatore Foti**: Investigation, Formal analysis. **Emiliano Giardina**: Investigation, Formal analysis. **Claudio De Felice**: Resources, Investigation. **Joussef Hayek**: Resources, Investigation. **Paolo Curatolo**: Resources, Investigation. **Cinzia Galasso**: Resources, Investigation. **Giuseppe Valacchi**: Resources, Investigation. **Massimiliano Coletta**: Conceptualization, Writing - original draft. **Grazia Graziani**: Conceptualization, Writing - original draft. **Stefano Marini**: Conceptualization, Writing - original draft.

Declaration of competing interest

The authors declare that they have no known competing financial interests or personal relationships that could have appeared to influence the work reported in this paper.

D

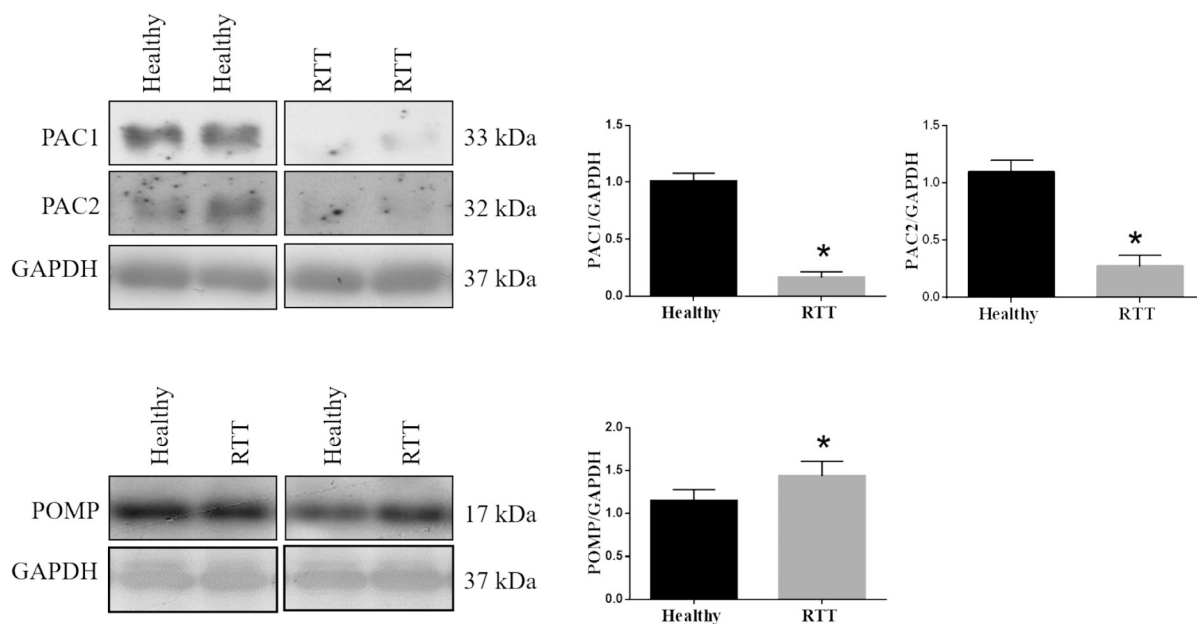


Fig. 3. (continued)

Acknowledgments

The authors acknowledge Dott. Alessio Cortelazzo (Chianciano, Italy) and prof. Cinzia Signorini (University of Siena, Siena, Italy) for their critical discussion during project execution and manuscript preparation. This study was funded by: PRIN 20157WZM8A and PRIN 2017SNRXH3 of MIUR and by Associazione Famiglie Rett, Italia.

Materials and methods

Cell lines isolation

RTT fibroblasts were isolated from patients enrolled in the study according to standard international criteria for diagnosis of the pathology as previously indicated, namely 3 of 6 main criteria (loss of hand skills, communication skills, and babble speech, hand stereotypes, deceleration of head growth, and a disease profile of regression followed by recovery of interaction) and 5 of 11 supportive criteria (periodic breathing, aerophagia, bruxism, apraxia of or no gait, scoliosis, lower limb muscle atrophy, cold feet, sleep disruption, inappropriate screaming/laughing, diminished nociception, and intense eye contact) [14,15,57]. Rett patients (8 and 12 years) bore the following *MECP2* mutations: R190fs (frame-shift), R255X. Normal fibroblasts were harvested from healthy subjects and matched for age (8 and 12 years) and gender (all subjects were females). Healthy and RTT fibroblasts were grown in complete DMEM supplemented with 10% FBS, nonessential amino-acids and antibiotics.

Native gel electrophoresis

The assay was performed by following methodology described elsewhere [44]. Crude cell extracts (e.g., soluble fraction of the cell) was extracted from cell pellets under non-denaturing condition through freeze-thawing cycles in 250 mM sucrose, 20% glycerol, 25 mM Tris-HCl, 5 mM MgCl₂, 1 mM EDTA, 1 mM DTT, 2 mM ATP, pH 7.4. Thereafter, lysates were cleared by centrifugation at 13,000 rpm, 20 min on ice and protein concentration normalized by Bradford assay. For each experimental condition, 75 µg of proteins were separated under native conditions into a 3.5% acrylamide gel. Remarkably, the

native-gel approach herein adopted visualizes protein complexes in the 3500 kDa 200 kDa range and the macromolecules are separated by their mass/charge. Inside gels, migration of the same assembly may be different depending on slightly different structural composition and post-translational decoration. Gels were then harvested and soaked in a clean dish in reaction buffer (50 mM Tris, 5 mM MgCl₂, 1 mM ATP, pH 7.5) supplemented with 100 µM 7-amino-4-methylcoumarin (AMC) labeled Suc - Leu - Leu - Val - Tyr -AMC peptide (referred to as LLVY-amc) specific for chymotrypsin-like activity of proteasome.

Proteins were then transferred to a HyBond-ECL nitrocellulose filters (see also below for details) and probed with an antibody specific proteasome subunits α7 or Rpn10 (Protein-tech), diluted 1:3000 in 0.02% Tween-PBS fat-free milk and, thereafter, incubated with a Horseradish Peroxidase-conjugated anti-rabbit or anti-mouse IgG antibody (Biorad, Hercules, CA, USA), diluted 1:50000 in 0.2% Tween-PBS fat-free milk.

Western blotting

For denaturing and reducing WB, cell pellets were lysed in RIPA buffer and cleared by centrifugation at 13,000 rpm for 30 min, at 4 °C. For each lane, a minimum of 15 µg of total proteins were loaded.

Proteins transfer to filters was done as described in the previous paragraph. The various antibodies used were administered following manufacturer indication (Abcam, Oxford, UK, Protein-tech) and developed as described in the previous section.

In-gel protein digestion

Excised bands were transferred to 1.5 mL microcentrifuge tubes and subjected to in-gel trypsin digestion. Briefly, the gel slices were destained, washed, reduced using 10 mM dithiothreitol (DTT), alkylated with iodoacetamide (IAA), and finally digested overnight at 37 °C with modified porcine trypsin. After in-gel digestion, the digested solution was transferred into a clean 0.5 mL tube. Peptides were extracted from gel pieces with 5% aqueous formic acid (FA) and subsequently with acetonitrile (CAN). This extraction procedure was repeated three times. The total extracts were pooled with the first supernatant and lyophilized. The recovered peptides were then reconstituted in 20 µL of water/acetonitrile (98:2) added with 5% FA.

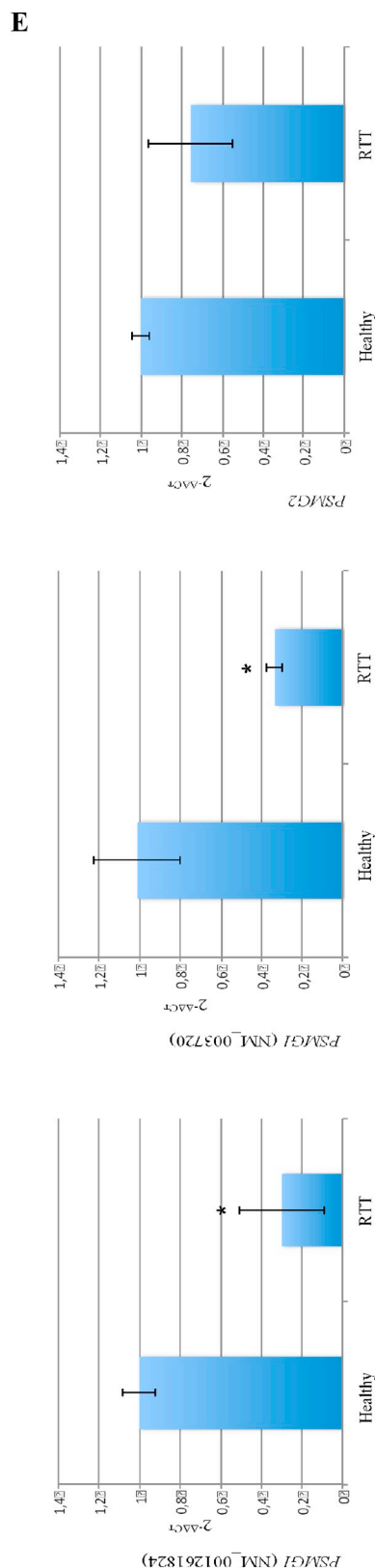


Fig. 3. (continued)

Mass spectrometry analysis

nLC-nESI MS/MS analysis was performed using a Thermo Scientific Dionex UltiMate 3000 RSLCnano system (Sunnyvale, CA) coupled online with a Thermo Fisher Scientific Orbitrap Fusion Tribrid® (Q-OT-

qIT) mass spectrometer (Thermo Fisher Scientific, Bremen, Germany). One microliter of the reconstituted tryptic peptide samples was loaded onto an Acclaim® Nano Trap C18 Column (100 $\mu\text{m} \times 2 \text{ cm}$, 5 μm , 100 \AA). After washing the trapping column with solvent A ($\text{H}_2\text{O}/\text{ACN}$, 98/2 + 0.1% FA) at a flow rate of 7 $\mu\text{L}/\text{min}$ for 3 min, the solution was switched from the trapping column onto a PepMap® RSLC C18 EASY-Spray column (75 $\mu\text{m} \times 50 \text{ cm}$, 2 μm , 100 \AA). Peptides were separated by elution at a flow rate of 0.25 $\mu\text{L}/\text{min}$ and 40 $^\circ\text{C}$ with a linear gradient of solvent B (ACN + 0.1% FA) in A from 5% to 20% in 35 min, followed by 20% to 40% in 30 min, 40% to 60% in 20 min, and 60% to 95% in another 5 min. We finished by holding 95% B for 5 min and re-equilibrating the column at 5% B for 20 min. Eluting peptide cations were converted to gas-phase ions by electrospray ionization using a source voltage of 1.9 kV and introduced into the mass spectrometer through a heated ion transfer tube (275 $^\circ\text{C}$). Survey scans of peptide precursors from 200 to 1600 m/z were performed at 120 K resolution (@ 200 m/z). Tandem MS was performed by isolation at 1.6 Th with the quadrupole, HCD fragmentation with normalized collision energy of 35, and rapid scan MS analysis in the ion trap. Only those precursors with charge state 2–4 and an intensity above the threshold of $5 \cdot 10^3$ were sampled for MS2. The dynamic exclusion duration was set to 60 s with a 10 ppm tolerance around the selected precursor and its isotopes. Monoisotopic precursor selection was turned on. The instrument was run in top speed mode with 3 s cycles, meaning that the instrument would continuously perform MS2 events until the list of non-excluded precursors diminishes to zero or 3 s, whichever is shorter. MS/MS spectral quality was enhanced enabling the parallelizable time option (*i.e.* by using all parallelizable time during full scan detection for MS/MS precursor injection and detection).

Mass spectrometer calibration was performed by using the Pierce® LTQ Velos ESI Positive Ion Calibration Solution (Thermo Fisher Scientific). MS data acquisition was carried out by utilizing the Xcalibur v. 3.0.63 software (Thermo Fisher Scientific).

Protein identification

LC/MS/MS data were analyzed and searched against the “human” SwissProt database (March 2017 release, containing 20,181 entries) using two different search engines: Mascot algorithm (Matrix Science, London, UK, version 2.5.1) and PEAKS *de novo* sequencing software (v. 8.5, Bioinformatics Solutions Inc., Waterloo, ON Canada). The amino acid sequences generated by PEAKS *de novo* sequencing software from each spectrum were searched using the SPIDER algorithm, a dedicated search tool of PEAKS that is specially designed to detect peptide mutations and perform cross-species homology search. For both search engines, the full tryptic peptides with a maximum of 3 missed cleavage sites were subjected to bioinformatic search. Cysteine carbamidomethylation was set as fixed modification, whereas oxidation of methionine, transformation of N-terminal glutamine and N-terminal glutamic acid residue in the pyroglutamic acid form, N-acetylation of N-terminus protein, acetylation of lysine, deamidation of glutamine and asparagine residues, and phosphorylation of serine, threonine and tyrosine residues were included as variable modifications. The precursor mass tolerance threshold was 10 ppm and the max fragment mass error was set to 0.6 Da.

Finally, all the protein hits obtained by these two approaches were processed by using the inChorus function of PEAKS. This tool combines the database search results of PEAKS software with those obtained by the Mascot search engine with the aim not only to increase the coverage, but also the confidence since the engines using independent algorithms and therefore confirm each other's results. Peptide spectral matches (PSMs) were validated if at least one of the following conditions was true: Mascot score ≥ 20 , PEAKS $-10\text{LogP} \geq 25$. The False Discovery Rate (FDR) values for PSMs, Peptide sequences and Proteins identified were always $\leq 0.2\%$. Only protein hits with a minimum of InChorus Protein score of 60% and at least one marker peptide,

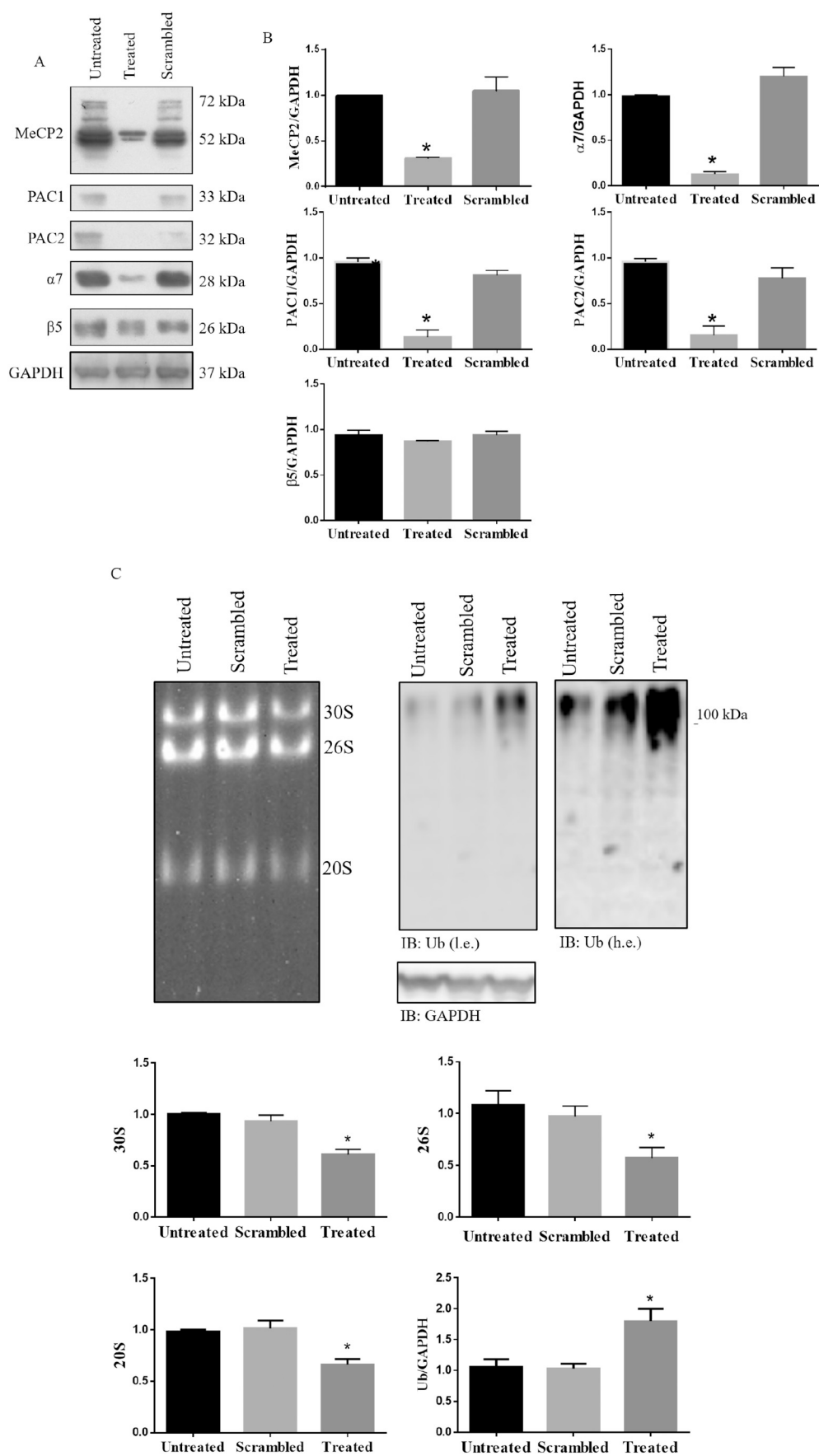


Fig. 4. MeCP2 silencing in SH-SY5Y cells recapitulates the proteasomal defect of RTT fibroblasts. MeCP2 expression was silenced upon delivery of 1 μ M antisense oligonucleotide (treated). As internal control, cells were either untreated or stimulated with 1 μ M non-targeting pool (scrambled). (A) semi-quantitative analysis of MeCP2, PAC1, PAC2, $\alpha 7$ and $\beta 5$ subunits of proteasome by denaturing and reducing WB; (B) Densitometric analysis, a nominal value of 1 was assigned to the protein/GAPDH ratio of untreated cells. * $p < 0.0001$ in all cases. Data are presented as mean \pm SEM. A representative blot of three independent experiments is shown. One-way ANOVA followed by Tukey's post-hoc significance test; (C) Native gel electrophoresis of proteasome particles isolated from the different experimental conditions. To improve detection of 20S, 0.05% SDS was administered in-gel. Poly-ubiquitinated proteins pattern as from denaturing and reducing WB is further provided. GAPDH was used as internal control. For densitometric analysis, a nominal value of 1 was assigned to 30S, 26S and 20S intensity along with staining of poly-ubiquitinated proteins in untreated cells. * $p < 0.001$ in all cases. Data are presented as mean \pm SEM. A representative blot of three independent experiments is shown. One-way ANOVA followed by Tukey's post-hoc significance test.

satisfying the above reported conditions, were considered valid.

Total RNA extraction and qPCR analysis

Total RNA was extracted from RTT and healthy primary human fibroblast cells using TRIzol Reagent (Life Technologies), according to the manufacturer's recommended procedure. The first-strand cDNA was obtained using a high capacity DNA reverse transcription kit (Applied Biosystems) according to the manufacturer's instructions [58]. Successively, the cDNA was subjected to qPCR assays which were performed using SYBR Green (Applied Biosystems) on a 7500 Fast Real Time PCR device (Applied Biosystems) [59]. Primer pairs were designed considering the following transcripts: *PSMG1* (NM_001261824; NM_003720), *PSMG2* (NM_020232), *PSMA3* (NM_002788), *PSMA7* (NM_002792), *PSMA2* (NM_002787), *PSMB1* (NM_002793), *PSMB5* (NM_002797) and *PSMC3* (NM_002804). Each reaction was run as triplicate and each assay was performed including a negative control. Relative mRNA expression levels of all examined genes were measured using the comparative $2^{-\Delta\Delta C_t}$ method, after normalizing to an endogenous reference gene (*GAPDH*). Furthermore, gene expression analysis was also performed using the Relative Quantitation (RQ) app on Thermo Fisher Cloud.

Ethical statement

All experimental protocols were approved by the Tor Vergata and Ferrara Universities Local ethic Committee all methodologies were carried out in accordance with relevant guidelines and regulations.

Informed consent was obtained from parents of children enrolled in the study.

References

- [1] R.E. Amir, I.B. Van den Veyver, M. Wan, C.Q. Tran, U. Francke, H.Y. Zoghbi, Rett syndrome is caused by mutations in X-linked MECP2, encoding methyl-CpG-binding protein 2, *Nat. Genet.* 23 (1999) 185–188, <https://doi.org/10.1038/13810>.
- [2] M. Chahrouh, S.Y. Jung, C. Shaw, X. Zhou, S.T.C. Wong, J. Qin, H.Y. Zoghbi, MECP2, a key contributor to neurological disease, activates and represses transcription, *Science*. 320 (2008) 1224–1229, <https://doi.org/10.1126/science.1153252>.
- [3] D.H. Yasui, S. Peddada, M.C. Bieda, R.O. Vallero, A. Hogart, R.P. Nagarajan, K.N. Thatcher, P.J. Farnham, J.M. Lasalle, Integrated epigenomic analyses of neuronal MeCP2 reveal a role for long-range interaction with active genes, *Proc. Natl. Acad. Sci. U. S. A.* 104 (2007) 19416–19421, <https://doi.org/10.1073/pnas.0707442104>.
- [4] L. Chen, C. Chen, L.A. Lavery, S.A. Baker, C.A. Shaw, W. Li, H.Y. Zoghbi, MeCP2 binds to non-CG methylated DNA as neurons mature, influencing transcription and the timing of onset for Rett syndrome, *Proc. Natl. Acad. Sci. U. S. A.* 112 (2015) 5509–5514, <https://doi.org/10.1073/pnas.1505909112>.
- [5] C.M. O'Driscoll, M.P. Lima, W.E. Kaufmann, J.P. Bressler, Methyl CpG binding protein 2 deficiency enhances expression of inflammatory cytokines by sustaining NF-kappaB signaling in myeloid derived cells, *J. Neuroimmunol.* 283 (2015) 23–29, <https://doi.org/10.1016/j.jneuroim.2015.04.005>.
- [6] A. Nott, J. Cheng, F. Gao, Y.-T. Lin, E. Gjoneska, T. Ko, P. Minhas, A.V. Zamudio, J. Meng, F. Zhang, P. Jin, L.-H. Tsai, Histone deacetylase 3 associates with MeCP2 to regulate FOXO and social behavior, *Nat. Neurosci.* 19 (2016) 1497–1505, <https://doi.org/10.1038/nn.4347>.
- [7] A. Cortelazzo, C. De Felice, R. Guerranti, C. Signorini, S. Leoncini, A. Pecorelli, G. Zollo, C. Landi, G. Valacchi, L. Ciccoli, L. Bini, J. Hayek, Subclinical inflammatory status in Rett syndrome, *Mediat. Inflamm.* 2014 (2014) 480980, <https://doi.org/10.1155/2014/480980>.
- [8] W.A. Gold, S.L. Williamson, S. Kaur, I.P. Hargreaves, J.M. Land, G.J. Pelka, P.P.L. Tam, J. Christodoulou, Mitochondrial dysfunction in the skeletal muscle of a mouse model of Rett syndrome (RTT): implications for the disease phenotype, *Mitochondrion*. 15 (2014) 10–17, <https://doi.org/10.1016/j.mito.2014.02.012>.
- [9] E. Cardaioli, M.T. Dotti, G. Hayek, M. Zappella, A. Federico, Studies on mitochondrial pathogenesis of Rett syndrome: ultrastructural data from skin and muscle biopsies and mutational analysis at mtDNA nucleotides 10463 and 2835, *J. Submicrosc. Cytol. Pathol.* 31 (1999) 301–304.
- [10] V. Conti, A. Gandaglia, F. Galli, M. Tirone, E. Bellini, L. Campana, C. Kilstrup-Nielsen, P. Rovere-Querini, S. Brunelli, N. Landsberger, MeCP2 affects skeletal muscle growth and morphology through non cell-autonomous mechanisms, *PLoS One* 10 (2015) e0130183, <https://doi.org/10.1371/journal.pone.0130183>.
- [11] M. Hara, T. Takahashi, C. Mitsumasa, S. Igata, M. Takano, T. Minami, H. Yasukawa, S. Okayama, K. Nakamura, Y. Okabe, E. Tanaka, G. Takemura, K. Kosai, Y. Yamashita, T. Matsuishi, Disturbance of cardiac gene expression and cardiomyocyte structure predisposes Mecp2-null mice to arrhythmias, *Sci. Rep.* 5 (2015) 11204, <https://doi.org/10.1038/srep11204>.
- [12] D. Jain, K. Singh, S. Chirumamilla, G.M. Bibat, M.E. Blue, S.R. Naidu, C.G. Eberhart, Ocular MECP2 protein expression in patients with and without Rett syndrome, *Pediatr. Neurol.* 43 (2010) 35–40, <https://doi.org/10.1016/j.pediatrneurol.2010.02.018>.
- [13] S.A. Rose, S. Wass, J.J. Jankowski, J.F. Feldman, A. Djukic, Impaired visual search in children with Rett syndrome, *Pediatr. Neurol.* 92 (2019) 26–31, <https://doi.org/10.1016/j.pediatrneurol.2018.10.002>.
- [14] A. Pecorelli, G. Leoni, F. Cervellati, R. Canali, C. Signorini, S. Leoncini, A. Cortelazzo, C. De Felice, L. Ciccoli, J. Hayek, G. Valacchi, Genes related to mitochondrial functions, protein degradation, and chromatin folding are differentially expressed in lymphomonocytes of Rett syndrome patients, *Mediat. Inflamm.* 2013 (2013) 137629, <https://doi.org/10.1155/2013/137629>.
- [15] F. Cervellati, C. Sticozzi, A. Romani, G. Belmonte, D. De Rasmio, A. Signorile, F. Cervellati, C. Milanese, P.G. Mastroberardino, A. Pecorelli, V. Savelli, H.J. Forman, J. Hayek, G. Valacchi, Impaired enzymatic defensive activity, mitochondrial dysfunction and proteasome activation are involved in RTT cell oxidative damage, *Biochim. Biophys. Acta* 1852 (2015) 2066–2074, <https://doi.org/10.1016/j.bbadis.2015.07.014>.
- [16] C. De Felice, F. Della Ragione, C. Signorini, S. Leoncini, A. Pecorelli, L. Ciccoli, F. Scalabri, F. Marracino, M. Madonna, G. Belmonte, L. Ricceri, B. De Filippis, G. Laviola, G. Valacchi, T. Durand, J.-M. Galano, C. Oger, A. Guy, V. Bultel-Poncé, J. Guy, S. Filosa, J. Hayek, M. D'Esposito, Oxidative brain damage in Mecp2-mutant murine models of Rett syndrome, *Neurobiol. Dis.* 68 (2014) 66–77, <https://doi.org/10.1016/j.nbd.2014.04.006>.
- [17] C. Signorini, S. Leoncini, C. De Felice, A. Pecorelli, I. Meloni, F. Ariani, F. Mari, S. Amabile, E. Paccagnini, M. Gentile, G. Belmonte, G. Zollo, G. Valacchi, T. Durand, J.-M. Galano, L. Ciccoli, A. Renieri, J. Hayek, Redox imbalance and morphological changes in skin fibroblasts in typical Rett syndrome, *Oxidative Med. Cell. Longev.* (2014), <https://doi.org/10.1155/2014/195935>.
- [18] L. Ciccoli, C. De Felice, S. Leoncini, C. Signorini, A. Cortelazzo, G. Zollo, A. Pecorelli, M. Rossi, J. Hayek, Red blood cells in Rett syndrome: oxidative stress, morphological changes and altered membrane organization, *Biol. Chem.* 396 (2015) 1233–1240, <https://doi.org/10.1515/hsz-2015-0117>.
- [19] C. Ciaccio, D. Di Pierro, D. Sbardella, G.R. Tundo, P. Curatolo, C. Galasso, M.E. Santarone, M. Casasco, P. Cozza, A. Cortelazzo, M. Rossi, C. De Felice, J. Hayek, M. Coletta, S. Marini, Oxygen exchange and energy metabolism in erythrocytes of Rett syndrome and their relationships with respiratory alterations, *Mol. Cell. Biochem.* 426 (2017) 205–213, <https://doi.org/10.1007/s11010-016-2893-9>.
- [20] S. Leoncini, C. De Felice, C. Signorini, G. Zollo, A. Cortelazzo, T. Durand, J.-M. Galano, R. Guerranti, M. Rossi, L. Ciccoli, J. Hayek, Cytokine dysregulation in MECP2- and CDKL5-related Rett syndrome: relationships with aberrant redox homeostasis, inflammation, and ω -3 PUFAs, *Oxidative Med. Cell. Longev.* 2015 (2015) 421624, <https://doi.org/10.1155/2015/421624>.
- [21] S.M. Kyle, P.K. Saha, H.M. Brown, L.C. Chan, M.J. Justice, MeCP2 co-ordinates liver lipid metabolism with the NCoR1/HDAC3 corepressor complex, *Hum. Mol. Genet.* 25 (2016) 3029–3041, <https://doi.org/10.1093/hmg/ddw156>.
- [22] S. Ricciardi, E.M. Boggio, S. Grosso, G. Lonetti, G. Forlani, G. Stefanelli, E. Calcagno, N. Morello, N. Landsberger, S. Biffo, T. Pizzorusso, M. Giustetto, V. Broccoli, Reduced AKT/mTOR signaling and protein synthesis dysregulation in a Rett syndrome animal model, *Hum. Mol. Genet.* 20 (2011) 1182–1196, <https://doi.org/10.1093/hmg/ddq563>.
- [23] S. Filosa, A. Pecorelli, M. D'Esposito, G. Valacchi, J. Hajek, Exploring the possible link between MeCP2 and oxidative stress in Rett syndrome, *Free Radic. Biol. Med.* 88 (2015) 81–90, <https://doi.org/10.1016/j.freeradbiomed.2015.04.019>.
- [24] D. Sbardella, G.R. Tundo, L. Campagnolo, G. Valacchi, A. Orlandi, P. Curatolo, G. Borsellino, M. D'Esposito, C. Ciaccio, S.D. Cesare, D.D. Pierro, C. Galasso, M.E. Santarone, J. Hayek, M. Coletta, S. Marini, Retention of Mitochondria in Mature Human Red Blood Cells as the Result of Autophagy Impairment in Rett Syndrome, *Sci. Rep.* 7 (1) (2017 Sep 26) 12297, <https://doi.org/10.1038/s41598-017-12069-0>.
- [25] J. Guy, J. Gan, J. Selfridge, S. Cobb, A. Bird, Reversal of neurological defects in a mouse model of Rett syndrome, *Science*. 315 (2007) 1143–1147, <https://doi.org/10.1126/science.1138389>.
- [26] M.H. Glickman, A. Ciechanover, The ubiquitin-proteasome proteolytic pathway: destruction for the sake of construction, *Physiol. Rev.* 82 (2002) 373–428, <https://doi.org/10.1152/physrev.00027.2001>.
- [27] A. Hershko, A. Ciechanover, The ubiquitin system, *Annu. Rev. Biochem.* 67 (1998) 425–479, <https://doi.org/10.1146/annurev.biochem.67.1.425>.
- [28] G.C. Lander, E. Estrin, M.E. Matyskiela, C. Bashore, E. Nogales, A. Martin, Complete subunit architecture of the proteasome regulatory particle, *Nature*. 482 (2012) 186–191, <https://doi.org/10.1038/nature10774>.
- [29] R.J. Tomko, M. Hochstrasser, Molecular architecture and assembly of the eukaryotic proteasome, *Annu. Rev. Biochem.* 82 (2013) 415–445, <https://doi.org/10.1146/annurev-biochem-060410-150257>.
- [30] G.R. Tundo, D. Sbardella, M. Coletta, Insights into proteasome conformation dynamics and intersubunit communication, *Trends Biochem. Sci.* 43 (2018) 852–853, <https://doi.org/10.1016/j.tibs.2018.08.002>.
- [31] Y. Hirano, K.B. Hendil, H. Yashiroda, S. Iemura, R. Nagane, Y. Hioki, T. Natsume, K. Tanaka, S. Murata, A heterodimeric complex that promotes the assembly of mammalian 20S proteasomes, *Nature*. 437 (2005) 1381–1385, <https://doi.org/10.1038/nature04106>.
- [32] Y. Hirano, H. Hayashi, S.-I. Iemura, K.B. Hendil, S.-I. Niwa, T. Kishimoto, M. Kasahara, T. Natsume, K. Tanaka, S. Murata, Cooperation of multiple chaperones

- required for the assembly of mammalian 20S proteasomes, *Mol. Cell* 24 (2006) 977–984, <https://doi.org/10.1016/j.molcel.2006.11.015>.
- [33] B. Le Tallec, M.-B. Barrault, R. Courbeyrette, R. Guérois, M.-C. Marsolier-Kergoat, A. Peyroche, 20S proteasome assembly is orchestrated by two distinct pairs of chaperones in yeast and in mammals, *Mol. Cell* 27 (2007) 660–674, <https://doi.org/10.1016/j.molcel.2007.06.025>.
- [34] S. Murata, H. Yashiroda, K. Tanaka, Molecular mechanisms of proteasome assembly, *Nat. Rev. Mol. Cell Biol.* 10 (2009) 104–115, <https://doi.org/10.1038/nrm2630>.
- [35] K. Sasaki, J. Hamazaki, M. Koike, Y. Hirano, M. Komatsu, Y. Uchiyama, K. Tanaka, S. Murata, PAC1 gene knockout reveals an essential role of chaperone-mediated 20S proteasome biogenesis and latent 20S proteasomes in cellular homeostasis, *Mol. Cell Biol.* 30 (2010) 3864–3874, <https://doi.org/10.1128/MCB.00216-10>.
- [36] K. Takagi, Y. Saeki, H. Yashiroda, H. Yagi, A. Kaiho, S. Murata, T. Yamane, K. Tanaka, T. Mizushima, K. Kato, Pba3-Pba4 heterodimer acts as a molecular matchmaker in proteasome α -ring formation, *Biochem. Biophys. Res. Commun.* 450 (2014) 1110–1114, <https://doi.org/10.1016/j.bbrc.2014.06.119>.
- [37] W. Wu, K. Sahara, S. Hirayama, X. Zhao, A. Watanabe, J. Hamazaki, H. Yashiroda, S. Murata, PAC1-PAC2 proteasome assembly chaperone retains the core α 4- α 7 assembly intermediates in the cytoplasm, *Genes Cells* 23 (2018) 839–848, <https://doi.org/10.1111/gtc.12631>.
- [38] B. Fricke, S. Heink, J. Steffen, P.-M. Kloetzel, E. Krüger, The proteasome maturation protein POMP facilitates major steps of 20S proteasome formation at the endoplasmic reticulum, *EMBO Rep.* 8 (2007) 1170–1175, <https://doi.org/10.1038/sj.embor.7401091>.
- [39] D. Sbardella, G.R. Tundo, F. Sciandra, M. Bozzi, M. Gioia, C. Ciaccio, U. Tarantino, A. Brancaccio, M. Coletta, S. Marini, Proteasome Activity Is Affected by Fluctuations in Insulin-Degrading Enzyme Distribution, *PLoS One* 10 (17) (2015 Jul 17) e0132455, <https://doi.org/10.1371/journal.pone.0132455> eCollection 2015.
- [40] D. Sbardella, G.R. Tundo, A. Coletta, J. Marcoux, E.I. Koufogeorgou, C. Ciaccio, A.M. Santoro, D. Milardi, G. Grasso, P. Cozza, M.-P. Bousquet-Dubouch, S. Marini, M. Coletta, The insulin-degrading enzyme is an allosteric modulator of the 20S proteasome and a potential competitor of the 19S, *Cell. Mol. Life Sci.* 75 (2018) 3441–3456, <https://doi.org/10.1007/s00018-018-2807-y>.
- [41] A.M. Santoro, A. Cunsolo, A. D'Urso, D. Sbardella, G.R. Tundo, C. Ciaccio, M. Coletta, D. Diana, R. Fattorusso, M. Persico, A. Di Dato, C. Fattorusso, D. Milardi, R. Purrello, Cationic porphyrins are tunable gatekeepers of the 20S proteasome, *Chem. Sci.* 7 (2016) 1286–1297, <https://doi.org/10.1039/c5sc03312h>.
- [42] K.J. Davies, Degradation of oxidized proteins by the 20S proteasome, *Biochimie* 83 (2001) 301–310, [https://doi.org/10.1016/s0300-9084\(01\)01250-0](https://doi.org/10.1016/s0300-9084(01)01250-0).
- [43] R. Raynes, L.C.D. Pomatto, K.J.A. Davies, Degradation of oxidized proteins by the proteasome: distinguishing between the 20S, 26S, and immunoproteasome proteolytic pathways, *Mol. Asp. Med.* 50 (2016) 41–55, <https://doi.org/10.1016/j.mam.2016.05.001>.
- [44] S. Elsasser, M. Schmidt, D. Finley, Characterization of the proteasome using native gel electrophoresis, *Methods Enzymol.* 398 (2005) 353–363, [https://doi.org/10.1016/S0076-6879\(05\)98029-4](https://doi.org/10.1016/S0076-6879(05)98029-4).
- [45] S. He, E. Barron, K. Ishikawa, H. Nazari Khanamiri, C. Spee, P. Zhou, S. Kase, Z. Wang, L.D. Dustin, D.R. Hinton, Inhibition of DNA methylation and methyl-CpG-binding protein 2 suppresses RPE Transdifferentiation: relevance to proliferative vitreoretinopathy, *Invest. Ophthalmol. Vis. Sci.* 56 (2015) 5579–5589, <https://doi.org/10.1167/iovs.14-16258>.
- [46] M. Ding, K. Shen, The role of the ubiquitin proteasome system in synapse remodeling and neurodegenerative diseases, *Bioessays* 30 (2008) 1075–1083, <https://doi.org/10.1002/bies.20843>.
- [47] T. Kishino, M. Lalande, J. Wagstaff, UBE3A/E6-AP mutations cause Angelman syndrome, *Nat. Genet.* 15 (1997) 70–73, <https://doi.org/10.1038/ng0197-70>.
- [48] T. Matsuura, J.S. Sutcliffe, P. Fang, R.J. Galjaard, Y.H. Jiang, C.S. Benton, J.M. Rommens, A.L. Beaudet, De novo truncating mutations in E6-AP ubiquitin-protein ligase gene (UBE3A) in Angelman syndrome, *Nat. Genet.* 15 (1997) 74–77, <https://doi.org/10.1038/ng0197-74>.
- [49] C.A. Chapleau, G.D. Calfa, M.C. Lane, A.J. Albertson, J.L. Larimore, S. Kudo, D.L. Armstrong, A.K. Percy, L. Pozzo-Miller, Dendritic spine pathologies in hippocampal pyramidal neurons from Rett syndrome brain and after expression of Rett-associated MECP2 mutations, *Neurobiol. Dis.* 35 (2009) 219–233, <https://doi.org/10.1016/j.nbd.2009.05.001>.
- [50] J.W. Murakami, E. Courchesne, R.H. Haas, G.A. Press, R. Yeung-Courchesne, Cerebellar and cerebral abnormalities in Rett syndrome: a quantitative MR analysis, *AJR Am. J. Roentgenol.* 159 (1992) 177–183, <https://doi.org/10.2214/ajr.159.1.1609693>.
- [51] V. Welk, O. Coux, V. Kleene, C. Abeza, D. Trümbach, O. Eickelberg, S. Meiners, Inhibition of proteasome activity induces formation of alternative proteasome complexes, *J. Biol. Chem.* 291 (2016) 13147–13159, <https://doi.org/10.1074/jbc.M116.717652>.
- [52] T. Kozai, T. Sekiguchi, T. Satoh, H. Yagi, K. Kato, T. Uchihashi, Two-step process for disassembly mechanism of proteasome α 7 homo-tetradecamer by α 6 revealed by high-speed atomic force microscopy, *Sci. Rep.* 7 (2017) 1–9, <https://doi.org/10.1038/s41598-017-15708-8>.
- [53] A.W. Khan, M. Ziemann, H. Rafahi, S. Maxwell, G.D. Ciccosto, A. El-Osta, MeCP2 interacts with chromosomal microRNAs in brain, *Epigenetics* 12 (2017) 1028–1037, <https://doi.org/10.1080/15592294.2017.1391429>.
- [54] A.A. de Jesus, A. Brehm, R. VanTries, P. Pillet, A.-S. Parentelli, G.A. Montealegre Sanchez, Z. Deng, I.K. Paut, R. Goldbach-Mansky, E. Krüger, Novel proteasome assembly chaperone mutations in PSMG2/PAC2 cause the autoinflammatory interferonopathy CANDLE/PRAAS4, *J. Allergy Clin. Immunol.* 143 (2019), <https://doi.org/10.1016/j.jaci.2018.12.1012> 1939–1943.e8.
- [55] M.C. Poli, F. Ebstein, S.K. Nicholas, M.M. de Guzman, L.R. Forbes, I.K. Chinn, E.M. Mace, T.P. Vogel, A.F. Carisey, F. Benavides, Z.H. Coban-Akdemir, R.A. Gibbs, S.N. Jhangiani, D.M. Muzny, C.M.B. Carvalho, D.A. Schady, M. Jain, J.A. Rosenfeld, L. Emrick, R.A. Lewis, B. Lee, Undiagnosed Diseases Network members, B.A. Zieba, S. Küry, E. Krüger, J.R. Lupski, B.L. Bostwick, J.S. Orange, Heterozygous truncating variants in POMP escape nonsense-mediated decay and cause a unique immune dysregulatory syndrome, *Am. J. Hum. Genet.* 102 (2018) 1126–1142, <https://doi.org/10.1016/j.ajhg.2018.04.010>.
- [56] M.G. Christ, H. Huesmann, H. Nagel, A. Kern, C. Behl, Sigma-1 receptor activation induces autophagy and increases proteostasis capacity in vitro and in vivo, *Cells* 8 (2019), <https://doi.org/10.3390/cells8030211>.
- [57] A.K. Percy, J.L. Neul, D.G. Glaze, K.J. Motil, S.A. Skinner, O. Khwaja, H.-S. Lee, J.B. Lane, J.O. Barrish, F. Annese, L. McNair, J. Graham, K. Barnes, Rett syndrome diagnostic criteria: lessons from the natural history study, *Ann. Neurol.* 68 (2010) 951–955, <https://doi.org/10.1002/ana.22154>.
- [58] R. Cascella, C. Strafella, M. Ragazzo, L. Manzo, G. Costanza, J. Bowes, U. Hüffmeier, S. Potenza, F. Sangiuolo, A. Reis, A. Barton, G. Novelli, A. Orlandi, E. Giardina, KIF3A and IL-4 are disease-specific biomarkers for psoriatic arthritis susceptibility, *Oncotarget* 8 (2017) 95401–95411, <https://doi.org/10.18632/oncotarget.20727>.
- [59] F. Ricci, G. Staurengi, T. Lepre, F. Missiroli, S. Zampatti, R. Cascella, P. Borgiani, L.T. Marsella, C.M. Eandi, A. Cusumano, G. Novelli, E. Giardina, Haplotypes in IL-8 gene are associated to age-related macular degeneration: a case-control study, *PLoS One* 8 (2013) e66978, <https://doi.org/10.1371/journal.pone.0066978>.